Am J Physiol Cell Physiol 293: C584–C596, 2007.
First published April 11, 2007; doi:10.1152/ajpcell.00600.2006.

Adverse effects of the classic antioxidant uric acid in adipocytes: NADPH oxidase-mediated oxidative/nitrosative stress

Yuri Y. Sautin, Takahiko Nakagawa, Sergey Zharikov, and Richard J. Johnson

Division of Nephrology, Hypertension, and Transplantation, Department of Medicine, University of Florida, Gainesville, Florida

Submitted 4 December 2006; accepted in final form 5 April 2007

Sautin YY, Nakawawa T, Zharikov S, Johnson RJ. Adverse effects of the classic antioxidant uric acid in adipocytes: NADPH oxidase-mediated oxidative/nitrosative stress. *Am J Physiol Cell Physiol* 293: C584–C596, 2007. First published April 11, 2007; doi:10.1152/ajpcell.00600.2006.—Uric acid is considered a major antioxidant in human blood that may protect against aging and oxidative stress. Despite its proposed protective properties, elevated levels of uric acid are commonly associated with increased risk for cardiovascular disease and mortality. Furthermore, recent experimental studies suggest that uric acid may have a causal role in hypertension and metabolic syndrome. All these conditions are thought to be mediated by oxidative stress. In this study we demonstrate that differentiation of cultured mouse adipocytes is associated with increased production of reactive oxygen species (ROS) and uptake of uric acid. Soluble uric acid stimulated an increase in NADPH oxidase activity and ROS production in mature adipocytes but not in preadipocytes. The stimulation of NADPH oxidase-dependent ROS by uric acid resulted in activation of MAP kinases p38 and ERK1/2, a decrease in nitric oxide bioavailability, and an increase in protein nitrosylation and lipid oxidation. Collectively, our results suggest that hyperuricemia induces redox-dependent signaling and oxidative stress in adipocytes. Since oxidative stress in the adipose tissue has recently been recognized as a major cause of insulin resistance and cardiovascular disease, hyperuricemia-induced alterations in oxidative homeostasis in the adipose tissue might play an important role in these derangements.

redox signaling; nitric oxide; reactive oxygen species

URIC ACID IS AN INTERMEDIATE product of the purine degradation pathway in the cell. In most mammals, uric acid is degraded further by the enzyme uricase. In humans and Great Apes, the uricase gene was inactivated during hominoid evolution (44), and uric acid is the final metabolic product of purine catabolism. Humans are unique among mammalian species by having the highest basal blood level of uric acid and the ability to develop hyperuricemia (22). Since the discovery in 1981 that urate is a powerful chemical antioxidant, which is present in human plasma in concentrations much higher than ascorbate (2), it is widely accepted that high blood levels of uric acid in humans carry an evolutionary advantage and that uric acid is a major antioxidant that protects cardiac, vascular, and neural cells from oxidative injury (14, 53).

On the other hand, hyperuricemia even without crystal deposition and gout is strongly associated with cardiovascular disease, kidney disease, and hypertension, increasing the risk of mortality (21). Hyperuricemia is also common in the metabolic syndrome and obesity (8, 37, 45). Albeit there is tremendous complexity of these disorders, an unambiguous common pathogenetic feature for all of them is, paradoxically, an involvement of oxidative stress and oxidative modifications of proteins and lipids as well as redox-dependent low-grade inflammation (5, 13, 18, 53, 57).

Oxidative stress and inflammation in the adipose tissue induce an imbalance in the production of adipocyte-specific hormones and cytokines (adipokines) that contribute substantially to the development of insulin resistance and cardiovascular risk associated with obesity (6, 13, 57). Serum levels of uric acid are positively correlated with obesity (8, 45), especially visceral obesity (37). Although hyperuricemia is often considered as a secondary phenomenon in the metabolic syndrome (50), it has also been noticed to be an independent predictor of obesity and hyperinsulinemia (42, 58). Most importantly, it has been shown recently that uric acid has a causal role in the metabolic syndrome induced by fructose (41). The possibility that uric acid could have a direct effect on the adipose tissue was not considered and to the best of our knowledge remains unknown.

Physiological concentrations of soluble microcrystal-free uric acid induce gene expression of chemokines and growth factors, such as monocyte chemoattractant protein (MCP)-1 and PDGF (24, 56), and stimulate proliferation of vascular smooth muscle cells (VSMC) (25). The effects of urate may involve complex and poorly understood redox-dependent pathways. Urate-induced MCP-1 expression in VSMC was attenuated by antioxidants, suggesting involvement of redox-dependent mechanism (24). Available data suggest that uric acid is not necessarily an antioxidant and, depending on the chemical milieu, may become a prooxidant. On one hand, in the extracellular environment, urate can scavenge hydroxyl radical, singlet oxygen, and peroxynitrite, especially when combined with ascorbic acid or thiols (1, 2, 31). On the other hand, uric acid loses its antioxidant ability in the hydrophobic environment (40). Moreover, it can form free radicals either alone (34) or in combination with peroxynitrite (51).

This study helps resolve the above paradox. We demonstrate that adipocyte differentiation is associated with increased uptake of uric acid and ROS accumulation and that elevated uric acid induced a further increase in intracellular ROS production in differentiated adipocytes, mediated by activation of NADPH oxidase (NOX). It is followed by redox-dependent stress signaling, a decrease in nitric oxide bioavailability, and oxidative modifications of proteins and lipids. Since oxidative stress in

Address for reprint requests and other correspondence: Y. Y. Sautin, Division of Nephrology, Hypertension, and Transplantation, Dept. of Medicine, Univ. of Florida, PO Box 100224, Gainesville, FL 32610-0224 (e-mail: sautiyy@medicine.ufl.edu).

The costs of publication of this article were defrayed in part by the payment of page charges. The article must therefore be hereby marked "*advertisement*" in accordance with 18 U.S.C. Section 1734 solely to indicate this fact.

adipose tissue has emerged as a major cause of insulin resistance and imbalance in vascular homeostasis, hyperuricemia-induced alterations in oxidative homeostasis in adipose tissue might play a crucial role in these derangements.

MATERIALS AND METHODS

Cell culture and treatments. Preadipocyte 3T3-L1 cells obtained from ATCC (Manassas, VA) were maintained in high-glucose DMEM (Invitrogen, Carlsbad, CA) supplemented with 10% FBS and antibiotics. For differentiation, we treated confluent cells with 10 μg/ml insulin, 0.25 μM dexamethasone, and 0.5 mM IBMX for 2 days, followed by 3-day treatment with insulin alone. Uric acid solution for cell treatments was prepared in the prewarmed cell culture medium (1–15 mg/dl Ultrapure, a microcrystal-free endotoxin-free solution; Sigma, St. Louis, MO) and passed through a 20-μm sterile filter, as previously described (24).

Detection of ROS and NO. We assessed intracellular ROS using several independent methods. *1*) We used the ROS-specific fluorescent probe 5(6)-chloromethyl-2′,7′-dichlorodihydrofluorescein diacetate-acetyl ester (CM-H_2DCFDA; Molecular Probes, Eugene, OR). At the end of treatments, cells were washed with Hanks' balanced salt solution (HBSS), followed by incubation in the presence of CM-H_2DCFDA (5 μM) for 30 min in HBSS. The cells were then transferred to the original growth medium, and green fluorescence was measured using an Axiovert 200 inverted microscope (Carl Zeiss). For image acquisition and analysis of fluorescence intensity, we used the LD Achroplan ×40/0.60 Corr objective (Carl Zeiss), the AxioCam MRm charge-coupled device camera (CCD), an FITC filter (excitation 480/30 nm, emission 535/40 nm), and AxioVision (v.4.5) image acquisition and analysis software. All optical filters were obtained from Chroma Technologies. Images were acquired every 5 min at ambient temperature for at least 45 min, and fluorescence intensity was measured in cytoplasmic regions of 20–30 cells per field in 3–4 fields per experiment. Preliminary experiments showed that fluorescence stabilized after incubation for about 30 min in the presence of CM-H_2DCFDA and remained stable for at least 15–20 min. Fluorescence intensities during this time interval were used for estimations of relative differences in ROS levels between groups. *2*) We also measured superoxide generation using nitroblue tetrazolium (NBT) assay (46). Briefly, at the end of treatments, 0.2% NBT (Sigma) was added to the medium for 1 h, followed by washing of the cell monolayer with PBS and dissolving of water-insoluble reduced NBT (blue formazan) accumulated in cells in 50% acetic acid. The absorbance of blue formazan was measured at 560 nm using the Bio-Tek Powerwave 200 microplate reader (Bio-Tek Instruments, Winooski, VT). The contribution of the direct NBT reduction by uric acid in the culture medium to the total absorbance was negligible (~5% at the concentration 15 mg/dl when tested in the cell-free medium). *3*) We also detected superoxide using the lucigenin-enhanced chemiluminescence method (see below). *4*) We used Mn(II) tetrakis(1-methyl-4-pyridyl)porphyrin (MnTMPyP), a superoxide scavenger and a cell-permeable mimetic of superoxide dismutase, to distinguish superoxide from another ROS.

The intracellular level of nitric oxide (NO) was measured using the NO-specific fluorescent probe 4-amino-5-methylamino-2′,7′-difluorofluorescein diacetate (DAF-FM diacetate, 5 μM; Molecular Probes), following the same procedure as for ROS detection.

Immunofluorescence. For immunofluorescent detection of the $p40^{phox}$ and $p67^{phox}$ translocation or specific urate transporter URAT1 expression, we cultured cells on coverslips. After treatments, cells were fixed in 3% (wt/vol) paraformaldehyde in PBS, quenched in 50 mM ammonium chloride and treated with 0.1% Triton X-100 for 10 min. $p67^{phox}$ and $p40^{phox}$ were stained with affinity-purified goat polyclonal NH_2-terminal antibodies for $p67^{phox}$ (N-19) and $p40^{phox}$ (N-20; Santa Cruz Biotechnology, Santa Cruz, CA) or URAT1 COOH-terminal polyclonal antibody (Alpha Diagnostics International, San Antonio, TX) overnight at 4°C, followed by incubation with FITC-conjugated donkey anti-goat or anti-rabbit IgG, correspondingly (1:50; Santa Cruz Biotechnology) for 45 min. Nuclei were counterstained with 4,6-diamidino-2-phenylindole.

Examination of immunolocalization and translocation of $p67^{phox}$ and $p40^{phox}$ by optical sectioning and three-dimensional deconvolution. The slides obtained by immunofluorescent staining with $p40^{phox}$ monoclonal antibody were examined using a ×63 oil-immersion Plan-Apochromat ×63/1.4 objective under an Axioplan 2 imaging microscope (Carl Zeiss). Optical Z-sectioning and three-dimensional deconvolution (constrained iterative method) of the optical sections was performed using image acquisition and analysis software AxioVision (v.4.5).

Measurement of NADPH oxidase. NADPH oxidase activity was measured using the lucigenin-enhanced chemiluminescence method in crude cell homogenates and microsomal membrane fractions by following previously described procedures with minor modifications (15, 54). To prepare cell homogenates, the cell monolayer was washed three times with ice-cold PBS and scraped on ice in lysis buffer containing 20 mM K-phosphate buffer (pH 7.0), 1 mM EGTA, 1 mM PMSF, 10 μg/ml aprotinin, and 5 μg/ml leupeptin, followed by homogenization with 100 strokes in a Dounce homogenizer on ice. For the isolation of microsomal membranes, cell homogenates were prepared in 250 mM sucrose, 5 mM HEPES (pH 7.4), 1 mM PMSF, 10 μg/ml aprotinin, and 5 μg/ml leupeptin, followed by centrifugation at 1,000 *g* (10 min, 4°C). The pellet was discarded, and the supernatant was spun at 8,000 *g* (10 min, 4°C). The microsomal fraction was separated from cytosol by centrifugation of the supernatant at 105,000 *g* (45 min, 4°C). The pellet was resuspended in the homogenization buffer by using a Hamilton glass syringe. The cell homogenate and microsomal fraction were used immediately. The assay was started in an Orion microplate luminometer (Berthold Detection Systems) by automatic injection of the 150-μl reaction buffer [50 mM K-phosphate buffer (pH 7.0) containing 1 mM EGTA, 150 mM sucrose, 5 μM lucigenin, and 100 μM NADPH] into 10 μl of the homogenate or membrane suspension (5–20 μg protein). Photon emission in response to superoxide generation was measured every 60 s with a 5-s signal integration time for 20 min. The activity is expressed in relative light units per milligram of protein. The protein concentration was measured using the bicinchoninic acid protein assay (Pierce, Rockford IL).

Immunoblot detection of $p67^{phox}$, $p40^{phox}$, and phosphorylation of p38 and ERK1/2. Phosphorylated and total p38 and ERK1/2 were detected by Western blotting with phosphorylation state-specific antibodies for p38 and ERK1/2 obtained from Cell Signaling Technology (Beverly, MA). $p67^{phox}$ and $p40^{phox}$ were detected with affinity-purified goat polyclonal antibodies from Santa Cruz Biotechnology. GAPDH was detected with monoclonal antibodies from Chemicon (Temecula, CA). Cells were rinsed twice with ice-cold PBS following treatment and scraped into ice-cold buffer containing 50 mM Tris·HCl (pH 7.6), 120 mM NaCl, 1% Nonidet P-40, 10% glycerol, 1 mM PMSF, 2 mM sodium orthovanadate, 10 mM sodium pyrophosphate, 40 μg/ml leupeptin, 5 μg/ml aprotinin, 1 μg/ml pepstatin, 100 mM NaF, 1 mM EDTA, and 1 mM EGTA. After lysis on ice for 60 min, extracts were centrifuged for 10 min at 14,000 *g* at 4°C. The protein concentration of the supernatants was measured, and 20-μg protein samples of cell lysate were mixed (1:1) with Laemmli sample buffer and incubated at 95°C for 5 min. Proteins were resolved by SDS-PAGE, followed by electroblotting onto polyvinylidene difluoride (PVDF) membrane. Membranes were blocked in 10 mM Tris (pH 7.5), 100 mM NaCl, and 0.1% Tween 20 containing 5% nonfat dry milk, followed by incubation with primary antibody. Membranes were washed three times and incubated with the appropriate horseradish peroxidase-conjugated secondary antibody. The immunocomplexes were visualized by chemiluminescence with the Phototope Western blot detection system (Cell Signaling Technology). The images were digitalized using the AlphaEase FluorChem digital imaging system (Alpha Innotech, San Leandro, CA). Band densitometry was per-

formed using NIH Image software. Ratios of phosphorylated kinases to total kinases or to housekeeping protein GAPDH were calculated.

Protein nitrosylation. To detect nitrosylated proteins, cell lysates were obtained as described above and proteins were resolved by SDS-PAGE, followed by electroblotting onto PVDF membrane. Nitrosylated proteins were detected by immunoblotting with monoclonal antibody to 3-nitrotyrosine (clone 39B6; Alexis Biochemicals, San Diego, CA). Densitometry of nitrosylated proteins was performed using NIH Image software.

Ratiometric fluorescent analysis of lipid oxidation with oxidation-sensitive lipid peroxidation probe C11-BODIPY$^{581/591}$. Lipid oxidation was measured using C11-BODIPY$^{581/591}$ (Molecular Probes), a validated lipid oxidation reporter molecule (9, 47). The probe accumulates readily in membrane and lipids, and in the presence of oxidized lipids its fluorescence shifts from red to green proportionally to the content of the oxidized lipids (9, 47). Differentiated adipocytes were incubated in HBSS in the presence of the probe (1 μM) for 30 min. The medium was then replaced with the HBSS-probe solution containing 7.5 mg/dl uric acid or vehicle. Time-lapse image capturing was started immediately following addition of uric acid at excitation/emission of 580/600 nm (the nonoxidized probe, red fluorescence) and at excitation/emission of 490/510 nm (the oxidized form, green fluorescence). For image acquisition, we used the LD A-Plan ×20 objective (Carl Zeiss) and the AxioCam MRm CCD camera. Time-lapse ratiometric image acquisition was performed every 60 s at ambient temperature using the ratio/FRET (fluorescence resonance energy transfer) module of SlideBook 4.1 software (Intelligent Imaging Innovations, Denver, CO). Exposure time for both green and red fluorescence was 100 ms in all experiments. Fluorescence intensity was measured in at least 12 regions of interest for each recording.

Real-time quantitative RT-PCR. Total RNA for quantification of mRNA expression for adiponectin and peroxisome proliferator-activated receptor (PPAR)-γ was extracted using Trizol reagent (Invitrogen). Trace DNA was removed using a DNA-free kit (Ambion, Austin, TX). Total RNA (1 μg) was converted to cDNA, and quantitative real-time RT-PCR was performed using the SuperScript III Platinum Two-Step qRT-PCR kit with SYBR green (Invitrogen) with primers optimized for real-time PCR: mouse PPAR-γ (designed based on GenBank accession no. NM_011146), 5′-GGAAAGACAACGGACAAATCA-3′ (forward) and 5′-AAACTGGCACCCTTGAAAAAT-3′ (reverse); mouse adiponectin (designed based on GenBank accession no. AF304466), 5′-AGGAGATGTTGGAATGACAGG-3′ (forward) and 5′-CTGAACGCTGAGCGATACATA-3′ (reverse). A 104-bp fragment of the mouse GAPDH was amplified simultaneously using the primers 5′-GGGTGTGAACCACGAGAAATA-3′ (forward) and 5′-AGTTGTCATGGATGACCTTGG-3′ (reverse). Real-time PCR was performed in the Opticon System (MJ Research) as follows: 94°C for 5 min, followed by 35 cycles of denaturation at 94°C for 30 s, annealing at 55°C for 1 min, and extension at 72°C for 90 s. Reaction specificity was confirmed by *1*) electrophoretic analysis of products in 2% agarose gel after real-time RT-PCR to check if bands of expected size were detected, *2*) melting curve analysis, and *3*) sequencing of amplified fragments. Ratios to GAPDH mRNA were calculated for each sample and expressed as means ± SD. Expression of adiponectin was additionally verified at the protein level by immunoblotting with monoclonal antibody for mouse adiponectin (clone MADI 1147; Alexis Biochemicals).

RT-PCR. URAT1 and subunits of the NADPH oxidase isoforms were detected by RT-PCR using SuperScript One-Step RT-PCR kit with Platinum Taq (Invitrogen). URAT1 was detected with a pair of primers amplifying a 170-bp fragment of the mouse URAT1 (GenBank NM_009203): 5′-ACAGAGGGTAGCTGCTGTCAA-3′ (forward) and 5′-ACAGCATGGAGATGATGGTTC-3′ (reverse). GAPDH was used as a housekeeping gene. A 104-bp fragment of the mouse GAPDH was amplified simultaneously with the primers described above. NOX subunits were detected using the following primer pairs: gp91^{phox} (NOX2; GenBank BC071229): 5′-AGGAGTGCCCAGTACCAAAGT-3′ (forward) and 5′-TACTGTCCCACCTCCATCTTG-3′ (reverse), 208 bp; NOX1 (GenBank NM_172203): 5′-AAAACTTCCTTTGGGAGACCA-3′ (forward) and 5′-CCAGACTCGAGTATCGCTGAC-3′ (reverse), 148 bp; NOX3 (GenBank NM_198958): 5′-GATGGCACCTGGACAGTACAT-3′ (forward) and 5′-TCTCCTGAGGCTCTGATGTGT-3′ (reverse), 126 bp; NOX4 (GenBank NM_015760): 5′-ACCCAAGTTCCAAGCTCATTT-3′ (forward) and 5′-ATGGTGACAGGTTTGTTGCTC-3′ (reverse), 114 bp; NOXA1 (GenBank NM_172204): 5′-GAGGCTGTGTCTGACTTCCAG-3′ (forward) and 5′-TGTGCTGATGCCATGTTGTAT-3′ (reverse), 128 bp; NOXA2 (GenBank NM_010877): 5′-CTGTCCGAAGAAAGCATGAAG-3′ (forward) and 5′-CTTAGGCTGAGGCTCCGTAGT-3′ (reverse), 159 bp; NOXO1 (GenBank NM_027988): 5′-GTGCTGGTCAGACAACAGTGA-3′ (forward) and 5′-AGGAAGCTTGGGAAGAACTTG-3′ (reverse), 139 bp; NOXO2 (GenBank NM_010876): 5′-GCCATTGCTGACTACGAGAAG-3′ (forward) and 5′-TTGTCTTCATCTGGCAAAACC-3′ (reverse), 115 bp; p22^{phox} (GenBank NM_007806): 5′-GCCATTGCCAGTGTGATCTAT-3′ (forward) and 5′-TCACACGACCTCATCTGTCAC-3′ (reverse), 237 bp; p40^{phox} (GenBank NM_007806): 5′-CACCAGCCACTTTGTTTTTGT-3′ (forward) and 5′-CTCAGCGATCTCTTGTTTTGC-3′ (reverse), 205 bp; DUOX1 (GenBank XM_983624): 5′-AATGCCAGTTGTCATTTCCAG-3′ (forward) and 5′-ATCTTGCATGTCCTCAACCAC-3′ (reverse), 195 bp; and DUOX2 (GenBank XM_988431): 5′-AGCAGTACAAGCGATTTGTGG-3′ (forward) and 5′-ACATGGTGAGCAGGATGTAGG-3′ (reverse), 219 bp. Reverse transcription was performed at 50°C for 30 min. The amplification step consisted of 30 or 35 cycles of denaturation at 94°C for 40 s, annealing for 1 min at 55°C, and extension of primers for 1 min at 72°C. The products were then held at 72°C for 5 min for DNA extensions to occur. Amplified fragments were separated by electrophoresis on 1% agarose gel, and the products were visualized by staining with 0.5 μg/ml ethidium bromide.

Urate uptake. Cells growing in 24-well plates were washed twice with a transport buffer containing 140 mM NaCl, 5.9 mM KCl, 1.2 mM $MgSO_4$, 2 mM Na_2HPO_4, 0.9 mM $CaCl_2$, 1 g/l glucose, and 10 mM HEPES-Tris buffer (pH 7.4). The mixture of unlabeled and radioactive [8-^{14}C]uric acid (50–60 mCi/mmol; American Radiolabeled Chemicals, St. Louis, MO) (total concentration varying from 50 to 500 μM) in the transport buffer was added to the cells to initiate transport assay, and the uptake was stopped 1–20 min later by extensive washing cells in ice-cold transport buffer. Radioactivity measured by liquid scintillation spectrometry was normalized for protein content.

Lipid detection. To visualize lipids, cells were washed with PBS, fixed in 3% paraformaldehyde, and stained with 0.3% Oil red O for 30 min. Triglyceride content in the cells was determined using a coupled enzymatic assay (Diagnostic Chemicals Limited, Oxford, CT).

Statistics. At least three independent experiments were performed in triplicate each. Data were analyzed using one-way ANOVA followed by Fisher's least significant test, unpaired Student's *t*-test, or Mann-Whitney *U*-test, with a value of $P < 0.05$ considered to represent a significant difference. Comparison between two values was performed by *t*-test or *U*-test. ANOVA was used to test differences among several means.

RESULTS

Increased ROS production and urate uptake are associated with the phenotype of differentiated adipocytes. We used a well-established model of 3T3-L1 mouse adipocytes (16). 3T3-L1 cells treated with the differentiation medium accumulated a remarkably high level of intracellular ROS, which is barely detectable in undifferentiated cells (Fig. 1*A*). As expected, adipocyte differentiation was associated with accumulation of lipids, increased expression of the adipogenic tran-

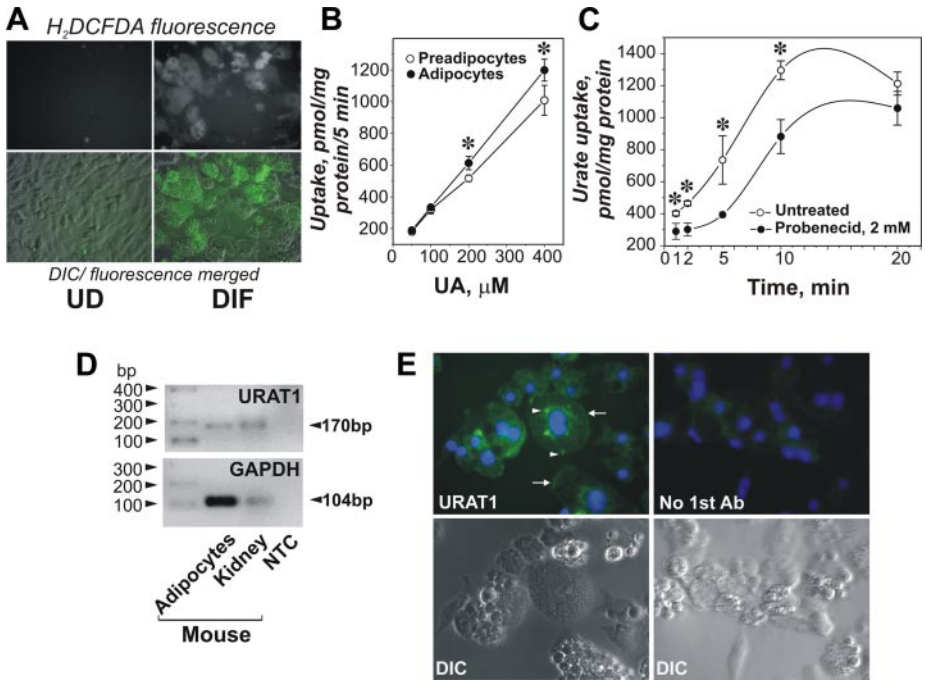

Fig. 1. Phenotype of differentiated adipocytes is associated with increased reactive oxygen species (ROS) production and uptake of uric acid (UA). *A*: ROS production by differentiated adipocytes (DIF) and preadipocytes (undifferentiated, UD). ROS were detected using live imaging with the fluorescent probe 5(6)-chloromethyl-2′,7′-dichlorodihydrofluorescein diacetate-acetyl ester (H_2DCFDA). ROS-induced fluorescence is shown at *top*; merged images of the fluorescence and differential interference contrast (DIC) are shown at *bottom*. *B*: uptake of [^{14}C]uric acid by 3T3-L1 cells (preadipocytes and differentiated adipocytes). Cells were incubated with the mixture of the labeled and nonradioactive uric acid (50–400 μM), and incorporated radioactivity was measured by scintillation counting. Values are means ± SD ($n = 4$). *$P < 0.05$ (*U*-test). *C*: effect of probenecid on uptake of [^{14}C]uric acid by 3T3-L1 cells (time course). Total urate concentration in the medium was 200 μM. Values are means ± SD ($n = 4$). *$P < 0.05$ (*U*-test). *D*: mRNA expression for URAT1 and GAPDH in adipocytes. Total RNA from differentiated adipocytes and kidneys of C57Bl6 mice (positive control) was analyzed by RT-PCR. Inverted images of agarose gels are shown. NTC, no-template control. *E*: immunofluorescent localization of URAT1 in differentiated adipocytes. Merged images of green (URAT1 immunoreactivity) and blue (4,6-diamidino-2-phenylindole, DAPI) fluorescence are shown at *top*. DIC images are shown at *bottom*. Membrane and vesicular localization of URAT1 is indicated by arrows and arrowheads, respectively.

scription factor (PPAR-γ), and the adipocyte-specific hormone adiponectin (see Supplemental Fig. S1; supplemental data for this article is available online at the *American Journal of Physiology-Cell Physiology* website).

3T3-L1 adipocytes demonstrated a rapid uptake of [^{14}C]uric acid (Fig. 1, *B* and *C*). The uptake rate in differentiated adipocytes was significantly higher than in undifferentiated cells (Fig. 1*B*). Probenecid, an inhibitor of urate transport via the organic anion transporter (OAT) family, including the specific urate transporter URAT1 (39), significantly attenuated urate uptake by adipocytes (Fig. 1*C*). RT-PCR for mouse URAT1 (Fig. 1*D*) and immunofluorescent detection of URAT1 (Fig. 1*E*) showed that differentiated adipocytes express this previously considered kidney-specific transporter with quite high intensity compared with the kidney. URAT1 was localized in the plasma membrane (Fig. 1*E*, arrows) and in vesicular structures in the perinuclear and plasma membrane regions (Fig. 1*E*, arrowheads). These data show that the mature adipocyte phenotype is associated with a high level of oxidant production, expression of a urate-specific transporter, and increased urate uptake.

Urate-induced production of ROS in adipocytes. Next, we determined whether the presence of soluble uric acid in the medium affects the level of ROS produced by adipocytes. Hyperuricemia in vivo is induced by a variety of causes and can be chronic or acute (26). To test long-term effects of uric acid, we incubated cells with varying concentrations of uric acid during adipocyte differentiation. To detect acute effects, uric acid was added to differentiated adipocytes for short periods of time (5–30 min). The presence of 1–15 mg/dl uric acid during the differentiation of adipocytes produced a moderate but significant increase in ROS production as determined using the NBT assay, whereas no effect of uric acid was detected in untreated undifferentiated cells or in incompletely differentiated cells (Fig. 2*A*). Similar results were obtained when ROS were detected using the fluorescent probe H_2DCFDA (Fig. 2, *B* and *C*). When differentiated adipocytes were treated with varying concentrations of uric acid for 30 min, the effect on ROS production was even more pronounced than after long-term stimulation (Fig. 2*D*). To determine whether transport of uric acid into adipocytes is required for stimulation of ROS production, we pretreated cells with probenecid and benzbromarone, two structurally unrelated OAT inhibitors of the transmembrane transport of urate (39). As shown in Fig. 2*E*, both inhibitors prevented stimulation of ROS generation in adipocytes in response to uric acid, suggesting that uric acid must enter the cell to induce ROS production.

Involvement of NADPH oxidase in urate-induced ROS production in adipocytes. One of the major sources of ROS and oxidative stress in many cells and tissues is an activation of nonphagocyte-type NADPH oxidase. In response to variety of stimuli, this enzyme generates superoxide anions ($O_2^{\bullet -}$), which are converted subsequently into other ROS (4, 7, 19, 32). To test whether uric acid-induced ROS are superoxide

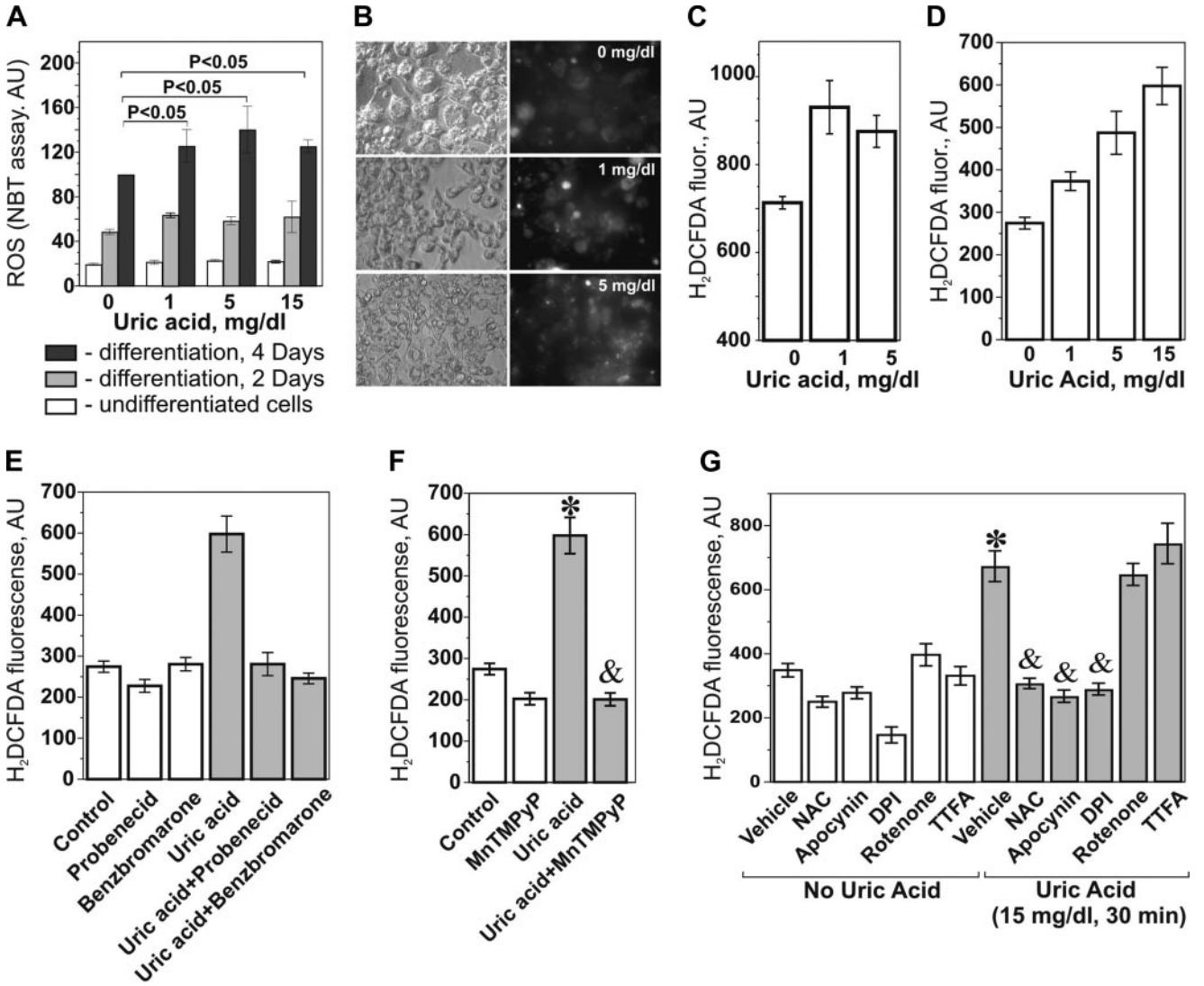

Fig. 2. Urate-induced NADPH oxidase-dependent ROS generation in 3T3-L1 adipocytes. *A*: long-term effect of uric acid [nitroblue tetrazolium (NBT) assay]. Values are means ± SD ($n = 3$ performed in triplicate). *B*: urate-induced ROS, long-term effect (H_2DCFDA). Images at *right*, fluorescence; images at *left*, phase contrast. *C*: image analysis of the fluorescence intensity shown in *B*. AU, arbitrary units. *D*: short-term effect of uric acid. Values are means ± SD ($n = 3$). The effect of uric acid is significant ($P < 0.05$, 1-way ANOVA). *E*: probenecid (1 mM) and benzbromarone (50 μM) added 30 min before cell stimulation prevented the effect of uric acid on ROS production. The effect of uric acid is significant ($P < 0.05$, *U*-test; $n = 3$). *F*: effect of Mn(II) tetrakis(1-methyl-4-pyridyl)porphyrin (MnTMPyP; 25 μM, 30-min preincubation) on urate-induced ROS. The effect of uric acid is significant (*$P < 0.05$, *U*-test). The effect of MnTMPyP is significant (&$P < 0.05$, *U*-test) compared with the uric acid-treated group ($n = 3$). *G*: apocynin and NOX inhibitors prevent urate-induced ROS production. The effect of uric acid is significant (*$P < 0.05$, *U*-test). The effect of the inhibitor is significant (&$P < 0.05$, *U*-test, $n = 3$). NAC, *N*-acetylcysteine; DPI, diphenylene iodonium; TTFA, thenoyltrifluoroacetone.

dependent, we treated cells with uric acid in the presence of 25 μM MnTMPyP, a cell-permeable mimetic of superoxide dismutase. MnTMPyP abolished the effect of uric acid on ROS production (Fig. 2*F*), demonstrating the involvement of superoxide in the urate-induced ROS generation. In addition, the effect of uric acid was completely blocked by the general antioxidant *N*-acetylcysteine (NAC; 10 mM) as well as by apocynin (200 μM) and diphenylene iodonium (10 μM), structurally unrelated NOX inhibitors, whereas rotenone (100 μM), an inhibitor of the mitochondrial electron transport chain complex I, and thenoyltrifluoroacetone (100 μM), an inhibitor of the complex II, were without effect (Fig. 2G). These data suggest that the elevation in ROS abundance in adipocytes in response to uric acid depends on superoxide generation by NADPH oxidase but not by the mitochondrial respiratory chain, another major source of superoxide in the cell.

Next, we examined the effect of uric acid on the enzymatic activity of NADPH oxidase. With the use of lucigenin-enhanced chemiluminescent superoxide detection, we found that cellular homogenates of differentiated adipocytes are capable of NADPH-dependent $O_2^{\bullet -}$ generation, which can be inhibited by apocynin or superoxide dismutase (Fig. 3*A*). These data indicate the presence of active NADPH oxidase in the adipocytes. Importantly, uric acid increased the superoxide dismutase-sensitive and apocynin-sensitive components of NADPH-dependent $O_2^{\bullet -}$ production in a dose-dependent manner (Fig. 3*B*). Since active NADPH oxidase is a membrane-associated enzyme (4, 7, 32), we tested the effect of uric acid

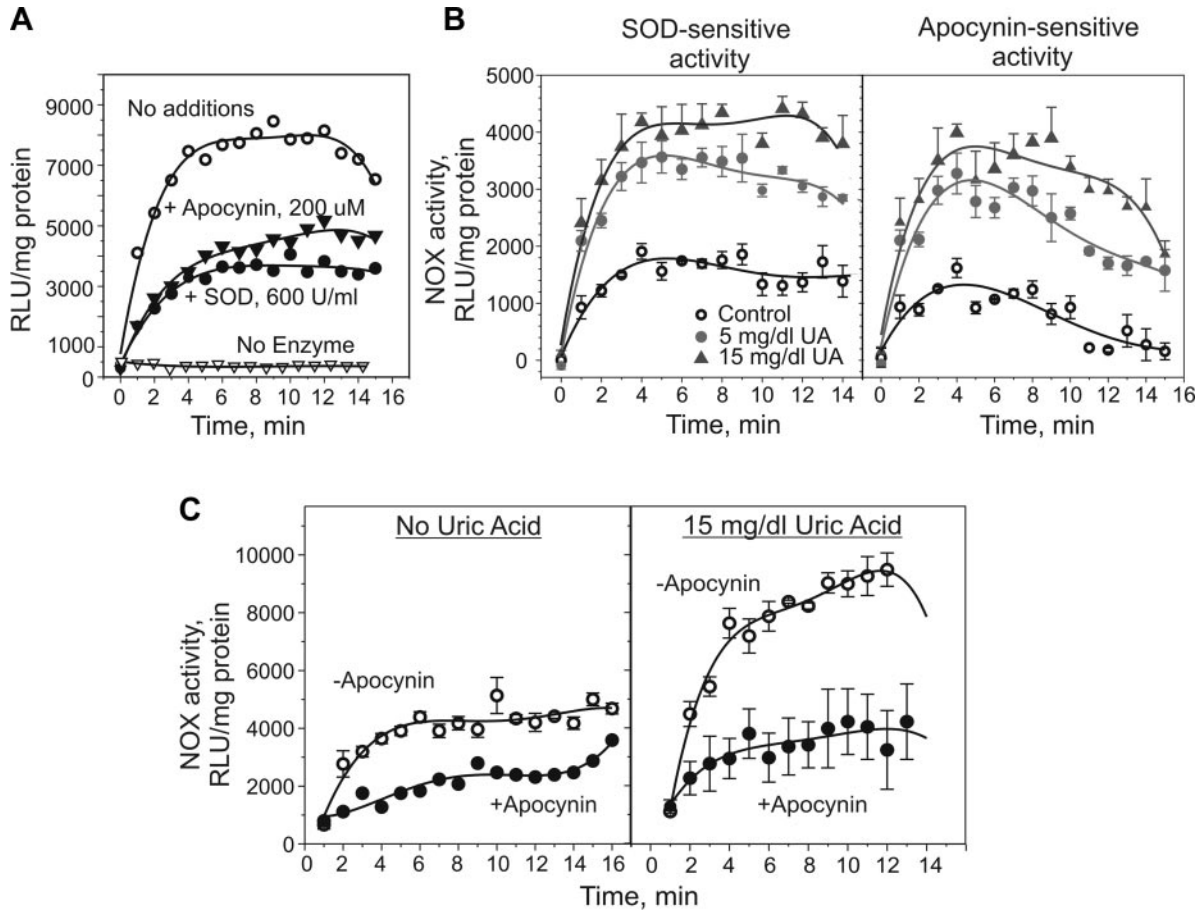

Fig. 3. Uric acid induces NADPH oxidase (NOX) activation in adipocytes. *A*: apocynin- and superoxide dismutase (SOD)-sensitive superoxide generation. RLU, relative light units. *B*: urate-induced increase in NOX activity in homogenates. Data are expressed as the difference of the total activity of the homogenate and the activity in the presence of SOD (600 U/ml) or apocynin (200 μM). Values are means ± SE ($n = 3$). *C*: urate-induced NOX activation in microsomal membranes. Values are means ± SE ($n = 3$).

on the NADPH oxidase activity in microsomal membranes. Treatment of differentiated adipocytes with uric acid stimulated apocynin-sensitive NADPH-dependent $O_2^{\bullet -}$ generation in the microsomal fraction (Fig. 3*C*).

The mechanism for the activation of NADPH oxidase-dependent ROS production depends on the nature of the particular NOX isoforms and subunits involved in the formation of the active holoenzyme (4, 7, 32). It is known that 3T3-L1 adipocytes express NOX4 (33). What kind of cytoplasmic regulatory subunits are expressed in these cells remains unknown, although NOX4, in contrast to other NADPH oxidases, does not require cytoplasmic proteins for its activity (35). To define the isoforms of NADPH oxidase in 3T3-L1 adipocytes and better understand potential mechanism(s) of NOX activation by uric acid, we analyzed expression of mRNA for most known isoforms of the NOX family as well as cytoplasmic regulatory subunits involved in the NOX activation (Fig. 4). Differentiated 3T3-L1 adipocytes predominantly express NOX4 (Fig. 4*A*), which is in agreement with the previously published observation (33). However, in addition to NOX4, we were able to detect NOX3 and NOX2 (gp91^{phox}) but not NOX1 (Fig. 4*A*), DUOX1, and DUOX2 (not shown). Among other proteins involved in the formation of active NADPH oxidase, we detected quite high expression of mRNAs for NOXA2 (p67^{phox}), NOXO1, and NOXO2 (p47^{phox}) (Fig. 4*B*). Expression of mRNA for p40^{phox} was lower than for other proteins, and this mRNA could be reliably detected only after increasing the number of amplification cycles (Fig. 4*C*). Surprisingly, p22^{phox}, which is an important activator for most NOX enzymes, was also detected only after additional amplification (Fig. 4, *B* and *C*), and it was expressed at a level comparable with p40^{phox}. Thus 3T3-L1 adipocytes express several isoforms of NADPH oxidase: NOX4, NOX3, and NOX2 with several regulatory subunits, including those involved in the formation of the classic phagocyte-type NADPH oxidase (gp91^{phox}, p67^{phox}, p47^{phox}, p40^{phox}, and p22^{phox}).

The predominant mechanism of activation for many NOX isoforms is a stimulus-induced assembly of the active holoenzyme on the plasma membrane (7, 32, 52). Since we observed an expression of p47^{phox} and p67^{phox}, which are required for the activation of gp91^{phox} and other NOX isoforms, and p40^{phox}, which also may play a regulatory role, we assessed the effect of uric acid on translocation of p67^{phox} and p40^{phox} to the membranes. Immunoblot analysis of subcellular fractions of adipocytes treated with uric acid revealed that uric acid induced a dramatic dose-dependent increase in the content of p67^{phox} in the microsomal fraction with a simultaneous decrease in the cytosol (Fig. 5*A*), indicating translocation of the subunit from the cytosol to membranes. An increase of p40^{phox} content in the microsomal fraction was also visible (Fig. 5*A*).

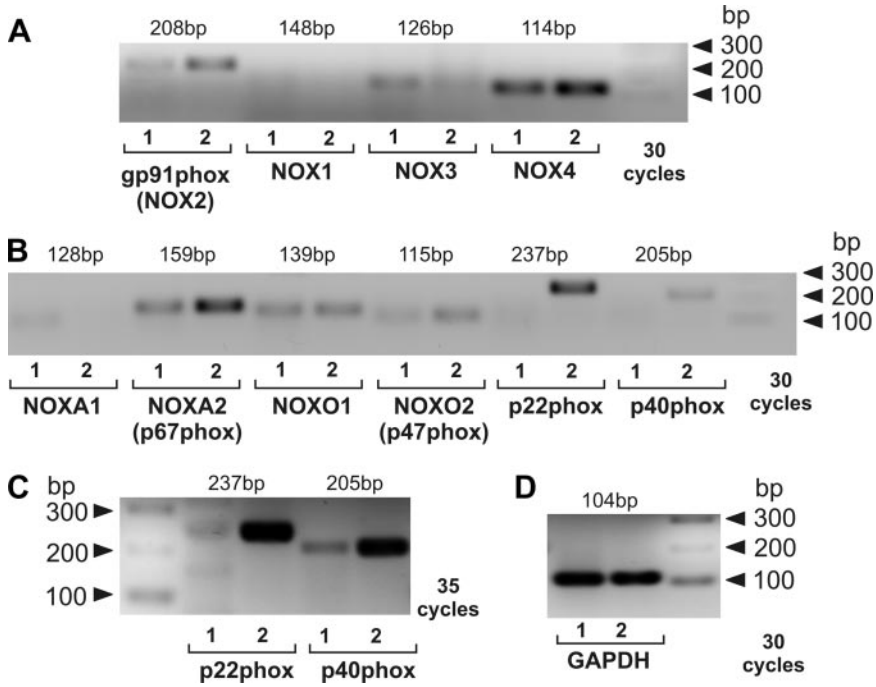

Fig. 4. Analysis of mRNA expression of NADPH oxidase isoforms and subunits in differentiated 3T3-L1 adipocytes. Total RNA was isolated from differentiated adipocytes, and, after treatment with DNase, 0.5 μg was amplified by RT-PCR with primers for all known mouse NOX isoforms and cytoplasmic subunits. Inverted images of agarose gels are shown; *lane 1*, adipocytes; *lane 2*, mouse kidney expressing many NADPH oxidases (positive control). Expected fragment size is shown above the gel image. *A*: NOX isoforms. *B*: cytoplasmic regulatory subunits with known isoforms. *C*: additional amplification of $p22^{phox}$ and $p40^{phox}$. *D*: amplification of the GAPDH fragment (housekeeping gene) of the same RNA.

However, immunodetection of this subunit was difficult because of the low expression. Membrane translocation of $p67^{phox}$ and $p40^{phox}$ upon stimulation with uric acid was further confirmed by characterization of the trafficking using immunofluorescent detection, followed by microscopy with optical sectioning and three-dimensional deconvolution of the optical sections. Figure 5*B* shows the diffuse cytoplasmic localization of $p67^{phox}$ and $p40^{phox}$ in untreated cells and the rapid translocation of the immunoreactivity to intracellular vesicular structures ($p67^{phox}$ and $p40^{phox}$) and to the plasma membrane ($p40^{phox}$).

Urate-induced redox-dependent activation of ERK1/2 and p38 MAP kinases is mediated by NADPH oxidase. ROS are pivotal components of intracellular signaling pathways and regulate a variety of normal cellular functions and/or stress response mechanisms and antioxidant systems. To test whether urate-induced NOX-dependent ROS production is involved in activation of intracellular signaling pathways, we examined the effect of uric acid on the activation of two major pathways: p38 MAP kinase and ERK1/2 MAP kinase. Uric acid rapidly induced a dramatic but transient increase in the amount of activated (phosphorylated) but not total p38 and ERK1/2 (Fig. 6*A*). The activation was maximal at 5 min and decreased to basal levels after 30 min. Similar manipulations with uric acid-free medium did not produce any changes in p38 and ERK1/2 phosphorylation (not shown), demonstrating that the activation is not a result of medium change. To test involvement of NADPH-dependent ROS, we pretreated adipocytes with NAC, MnTMPyP, or apocynin before stimulation with uric acid. The inhibitors did not produce statistically significant changes in the phosphorylation of p38 and ERK1/2 MAPKs under basal conditions, but MnTMPyP and apocynin abolished or at least significantly attenuated the effect of uric acid (Fig. 6*B*). However, the effect of NAC was not statistically significant. Since NAC is a precursor of glutathione, it suggests that redox-dependent activation of p38 and ERK1/2 MAP kinases by uric acid may be relatively independent of the status of the glutathione system. It has been reported previously that redox-dependent activation of MAP kinases might be glutathione (and NAC)-dependent in some cases (17) and independent in others (55). Overall, our data demonstrate that urate-induced activation of ERK1/2 and p38 is at least partially redox dependent and is mediated by NADPH oxidase-induced superoxide.

NADPH-dependent decrease in NO bioavailability in adipocytes in response to uric acid. A decrease in NO bioavailability in endothelial cells appears to play an important role in the pathway by which uric acid causes hypertension, metabolic syndrome, and kidney disease in experimental models (30, 41). Endothelial (eNOS)- and inducible NO synthase (iNOS)-dependent NO is abundant in adipocytes; however, the biological role of NO in these cells is considered important but remains incompletely understood (12, 28). To address the possibility of redox-dependent intracellular effects of uric acid on the NO system in adipocytes, we measured NO production in differentiated adipocytes treated with uric acid. The level of NO in differentiated adipocytes was much higher than in undifferentiated cells (Fig. 7*A*). An inhibitor of NO synthesis, N^{ω}-nitro-L-arginine methyl ester (L-NAME), attenuated DAF-FM fluorescence, demonstrating NOS-dependent NO production in adipocytes (Fig. 7*B*). Long-term cell treatment with uric acid during adipocyte differentiation induced a dose-dependent decrease in NO bioavailability to levels detected in preadipocytes (Fig. 7*C* and Supplemental Fig. S2). Undifferentiated cells were not affected by treatment with uric acid (Fig. 7*C*). Uric acid added to differentiated adipocytes also induced a rapid decrease in NO levels (Fig. 7*D* and Supplemental Fig. S3). Probenecid prevented this decrease, suggesting that the effect of uric acid required its transport into the cytoplasm (Fig. 7*D*). The decrease in NO bioavailability was not due to changes in eNOS activation mediated by phosphorylation of Ser1177 (Supplemental Fig. S3), suggesting that the mechanism for

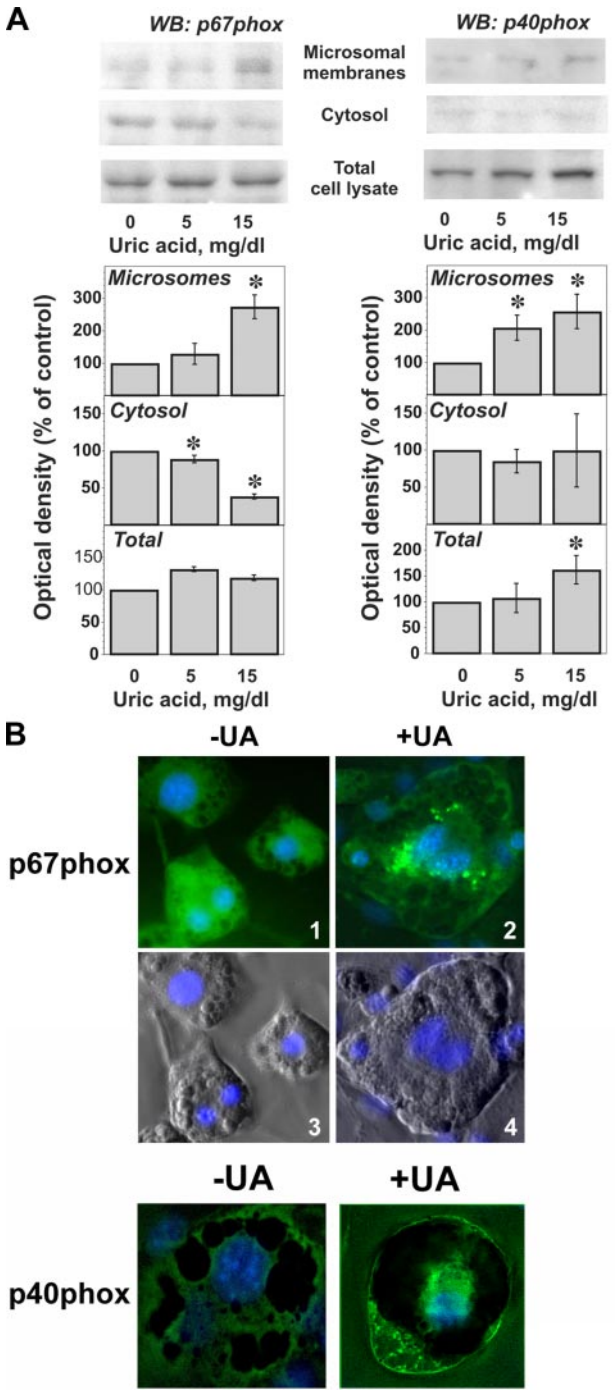

Fig. 5. Translocation of p67^{phox} and p40^{phox} in adipocytes in response to uric acid. Adipocytes were cultured and differentiated in 10-cm dishes (for cell fractionation) or on coverslips (for immunofluorescence). At the end of incubation with 5–15 mg/dl uric acid, cells were processed as described in MATERIALS AND METHODS. *A*: urate-induced changes in the content of p67^{phox} and p40^{phox} in microsomal fractions, cytosol, and total lysate. Densitometry values are changes in the optical density in response to uric acid, normalized to the corresponding control. *$P < 0.05$ compared with control (*U*-test, $n = 3$). WB, Western blot. *B*: effect of uric acid on p67^{phox} and p40^{phox} localization in adipocytes. Shown are 1-μm optical sections (*X*, *Y*). *Images 1* and *2*, immunofluorescence of p67^{phox}; *images 3* and *4*, merged images of DIC and DAPI staining to show nuclei.

reducing NO level is not related to the common signaling pathway for eNOS activation. The decrease in NO bioavailability in response to uric acid was attenuated by NAC and apocynin, demonstrating that the effect of uric acid is mediated by oxidants and activation of NADPH oxidase (Fig. 7*E*).

Uric acid-induced oxidative modifications in adipocytes: protein nitrosylation and lipid oxidation. Given the high basal level of NO in differentiated adipocytes (Fig. 7*A*), the effect of uric acid to induce a simultaneous increase in ROS production (Fig. 2) and decrease in NO bioavailability (Fig. 7) suggested that urate-induced overproduction of ROS might result in formation of peroxynitrite as well as other reactive nitrogen species. Once formed, these radicals can induce oxidative modifications of proteins and lipids. To test this possibility, we performed immunoblot detection of nitrosylated proteins in cell lysates obtained from adipocytes treated with uric acid by using monoclonal antibody to 3-nitrotyrosine. Nitration of tyrosine serves as a well-established marker or molecular "footprint" of reactive nitrogen species, including peroxynitrite (10). As shown in Fig. 8*A*, nitrosylated proteins are not detectable in untreated adipocytes, whereas long-term exposure to 1–15 mg/dl uric acid increased the amount of several nitrosylated proteins starting with the lowest tested concentration (Fig. 8*A*, *bands 1–5*) to detectable levels. Treatment of adipocytes with uric acid for 30 min increased nitrosylation of the protein(s) (Fig. 8*B*) with the apparent molecular mass similar to that of *protein 2* detected after long-term stimulation with uric acid (Fig. 8*A*). Cell pretreatment with NAC, MnTMPyP, or apocynin prevented nitrosylation of this protein (Fig. 8*B*). Thus superoxide generation and active NADPH oxidase are responsible for uric acid-induced protein nitrosylation in adipocytes.

To test formation of oxidized lipids, we used the oxidation-sensitive fluorescent fatty acid analog C11-BODIPY$^{581/591}$, which accumulates in lipid-containing structures of the cell and shifts fluorescence from red to green upon lipid peroxidation (9, 47). Green fluorescence of the probe as well as green/red fluorescence ratio gradually increased in untreated adipocytes, most likely because of high basal level of oxidants (Fig. 8, *C* and *D*). Uric acid induced a dramatic increase in green fluorescence of the probe almost immediately, and this increase continued for at least 45–60 min (Fig. 8, *C* and *D*, and Supplemental Fig. S4b) becoming visible after long-term treatment (Supplemental Fig. S4a). This effect was completely blocked by MnTMPyP or apocynin (Fig. 8, *C*and *D*), demonstrating that lipid oxidation in response to uric acid was mediated by NOX-dependent superoxide.

DISCUSSION

The presented study is the first demonstration that uric acid exerts direct effects in adipocytes with potentially very important implications for our understanding of causal factors of the metabolic syndrome. It also provides a possible explanation for the paradox in which the chemical antioxidant urate is associated with diseases driven by oxidative stress. We have demonstrated that, at least in adipocytes, the redox-dependent effects of uric acid are mediated not by the redox chemistry of the urate compound but by the activation of intracellular oxidant production via NADPH oxidase.

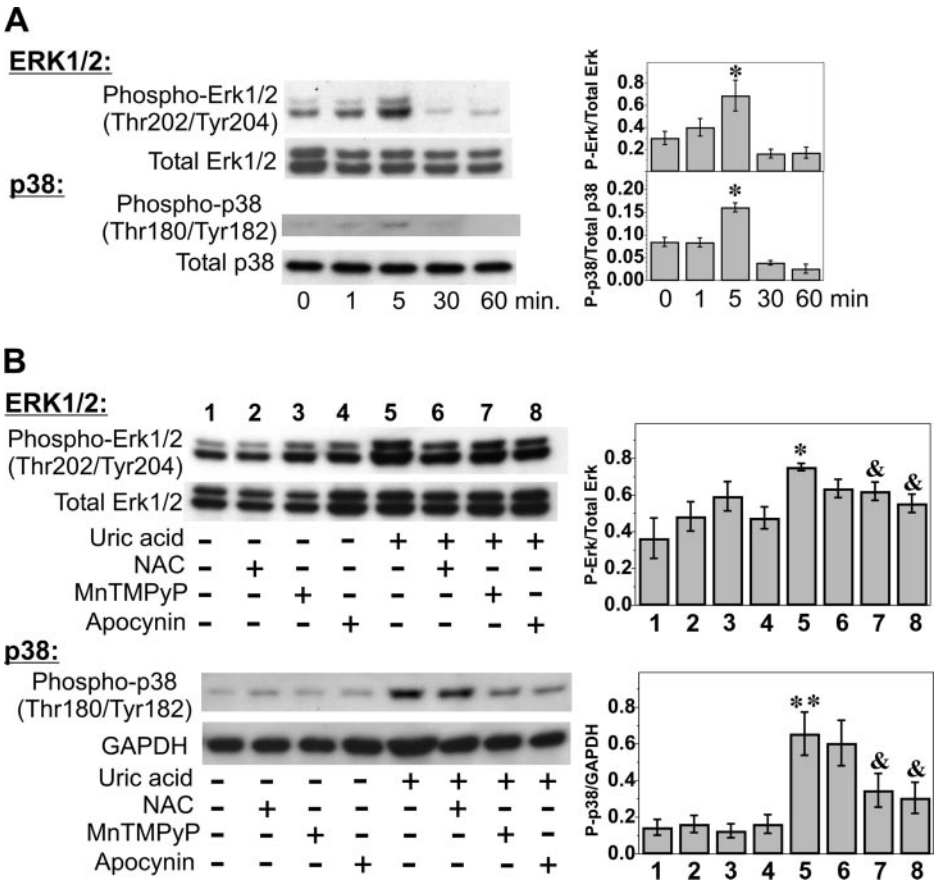

Fig. 6. Redox-dependent activation of p38 and ERK1/2 MAP kinases in adipocytes in response to uric acid is mediated by NADPH oxidase. Adipocytes were treated with 15 mg/dl uric acid for varying periods of time with or without antioxidants or an inhibitor of NADPH oxidase. *A*: time course for phosphorylation (P) of ERK1/2 and p38 in response to uric acid in adipocytes. *B*: urate-induced ERK1/2 and p38 phosphorylation is redox dependent and mediated by NOX. Images were digitalized, and the optical density of the bands was analyzed using NIH Image software. Values are ratios of the content of phosphorylated and total kinases for 3 blots (±SD). *$P < 0.05$ compared with control (*U*-test, $n = 3$) &$P < 0.05$ compared with no. 5 (uric acid alone) (*U*-test; $n = 3$).

So far, direct effects of soluble uric acid were characterized mostly in vascular smooth muscle cells and endothelial cells. In VSMC, uric acid activates critical proinflammatory pathways (23, 24) and stimulates cell proliferation (25, 49). In endothelial cells, uric acid decreases NO bioavailability (27, 30) and inhibits cell migration and proliferation, which are mediated in part by the expression of C-reactive protein (27).

We observed urate-induced NADPH oxidase-dependent augmentation of ROS production and downstream ROS-mediated effects in differentiated adipocytes but not in preadipocytes. Adipocyte differentiation itself, which is accompanied by lipid accumulation and expression of differentiation markers in 3T3-L1 cells, induced basal ROS production, confirming recent findings (13). In addition, adipocyte differentiation enhanced the capacity of the adipocyte to uptake uric acid. Surprisingly, URAT1, previously considered as a kidney-specific urate transporter (39), is expressed in adipocytes and may be one of the transporters of uric acid in these cells. URAT1 is also expressed by the human vascular smooth muscle cell (48). The observation that ROS production in response to uric acid and downstream redox-dependent effects is sensitive to blockade of urate transport with probenecid and benzbromarone suggests that entry of uric acid into the cell is required for these effects.

The long-term and short-term effects of uric acid are similar. We observed dose-dependent effects of uric acid in our in vitro model of hyperuricemia in mouse adipocytes within a concentration range of 1–15 mg/dl, with distinct effects observed at concentrations as low as 1 mg/dl (60 μM). Mice, like most mammals, have active uricase eliminating most produced uric acid. Humans are not able to maintain the level of uric acid lower than about 3 mg/dl (20). Therefore, it is possible that the dose dependence of the effects of uric acid in human adipocytes will be different.

Uric acid induced activation of NADPH oxidase in crude homogenates and isolated microsomal membranes of adipocytes. Mechanisms of activation of NOX enzymes vary greatly depending on the spectrum of expressed isoforms and cytoplasmic regulators. NOX1–NOX3 require the presence of $p22^{phox}$ on the membrane and are more or less dependent on cytoplasmic subunits $p47^{phox}$, $p67^{phox}$, and $p40^{phox}$, which translocate to the membrane and form with NOX and $p22^{phox}$ an active holoenzyme complex in response to cell stimulation (4, 32). NOX4 is a $p22^{phox}$-dependent enzyme but does not require cytoplasmic subunits (35), and neither of these subunits is involved in the activation of NOX5 (4). Analysis of the mRNA expression for known isoforms of NADPH oxidase presented in this study revealed that differentiated adipocytes express NOX2, NOX3, and NOX4 as well as different types of cytosolic subunits, including $p67^{phox}$ and $p47^{phox}$, which can activate several NOX enzymes. mRNA for $p22^{phox}$, an important stabilizer for most NADPH holoenzymes, and $p40^{phox}$, which is involved together with $p47^{phox}$ in the binding of 3-phosphoinositol lipids (11, 38), are also expressed in 3T3-L1 adipocytes at lower levels. Such a diversity in the expression of NOX isoforms can be explained by the homology of adipocytes with phagocytes (expression of $gp91^{phox}$), the embryonic origin of 3T3-L1 cells [expression of NOX3, which is abun-

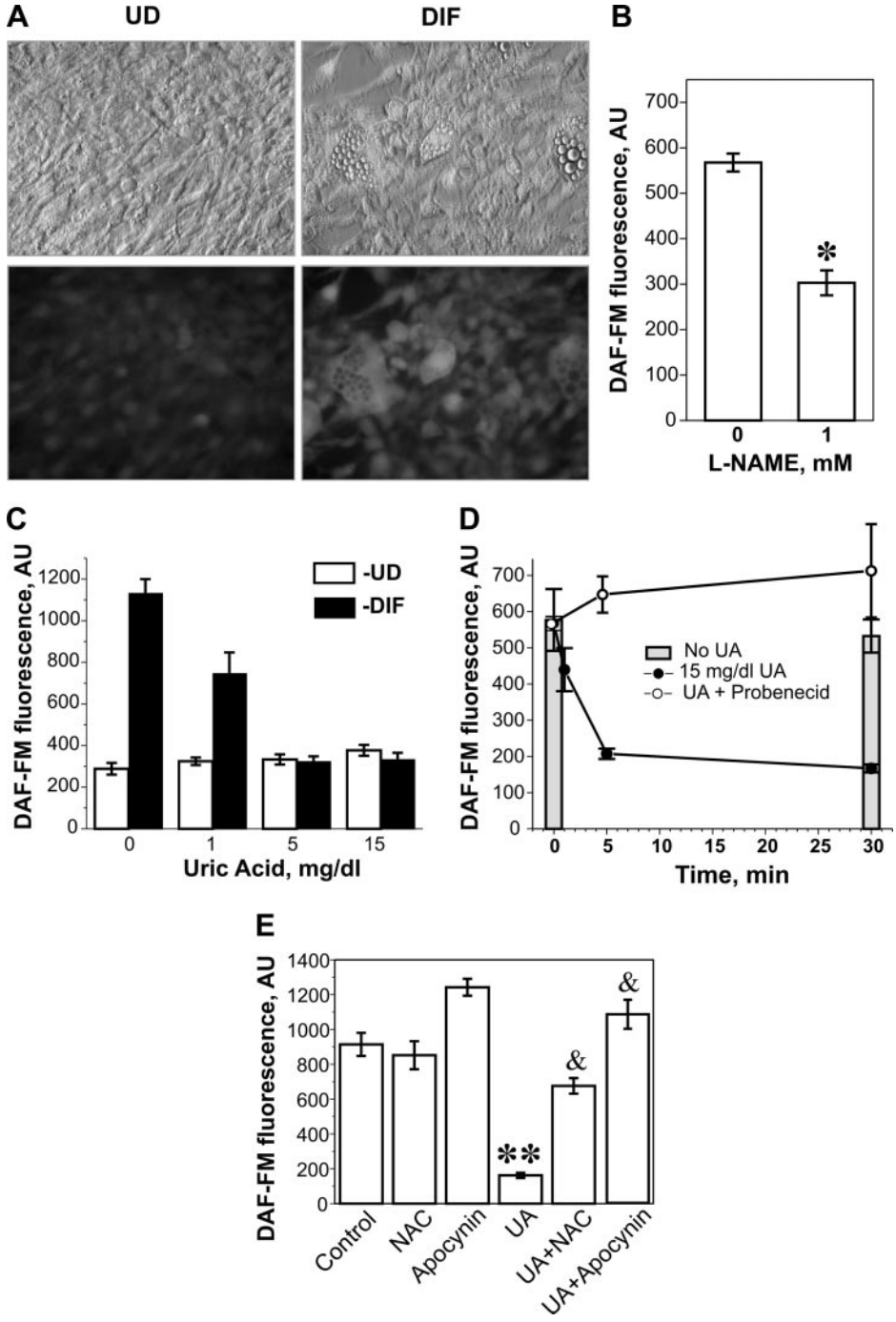

Fig. 7. Uric acid induces NOX-dependent decrease in NO bioavailability in adipocytes. *A*: nitric oxide (NO) induced fluorescence of the 4-amino-5-methylamino-2′,7′-difluorofluorescein diacetate (DAF-FM) probe. Images at *top*, phase contrast; images at *bottom*, fluorescence. *B*: suppression of NO production in adipocytes with N^{ω}-nitro-L-arginine methyl ester (L-NAME). Cells were treated with L-NAME for 30 min before live imaging of NO production. Values are means ± SD ($n = 3$). *$P < 0.05$ (*t*-test). *C*: urate-induced decrease in NO bioavailability. 3T3-L1 cells were differentiated into adipocytes or incubated without differentiation factors in the presence or absence of varying concentrations of uric acid. Values are means ± SD ($n = 3$). The effect of uric acid is significant ($P < 0.05$, 1-way ANOVA). *D*: probenecid-sensitive acute effect of uric acid on NO bioavailability. Cells were pretreated with 1 mM probenecid for 30 min before addition of uric acid. Values are means ± SD ($n = 3$). The effect of uric acid is significant ($P < 0.05$, 1-way ANOVA). *E*: urate-induced decrease in NO bioavailability in adipocytes is prevented by antioxidants and inhibition of NOX. Cells were treated with 10 mM NAC or 200 μM apocynin for 30 min before addition of uric acid. **$P < 0.01$ compared with untreated cells (*U*-test). &$P < 0.05$ compared with urate-treated group (*U*-test, $n = 3$).

dant in fetal tissues (4, 32)], and the ubiquity of NOX4. These NOX isoforms can provide constitutive and stimulated ROS production in adipocytes, and different mechanisms may be involved in the activation of NADPH oxidase in response to stimulation. Our data on translocation of $p67^{phox}$ and $p40^{phox}$ in response to uric acid indicate the possibility of assembly of the classic phagocyte-type NADPH oxidase based on $gp91^{phox}$ or another NOX protein. Because we observed an increase in the content of $p40^{phox}$, and because of the abundance of NOX4 in adipocytes, which is regulated predominantly at the level of transcription (4), the mechanisms underlying regulation of NOX expression are a promising topic for future experiments. The upstream signaling mechanism linking urate transport into the cell and formation of the active NOX complex in adipocytes remain largely unknown.

NOX-dependent superoxide generation in adipocytes induced in response to uric acid is associated with an increase in phosphorylation of p38 and ERK1/2, which can be blocked, at least partially, by scavengers of superoxide and inhibitors of NADPH oxidase. This indicates that redox-dependent signaling via cascades of MAP kinases mediates the effects of uric acid in adipocytes downstream from NADPH oxidase. Activation of p38 and ERK1/2 in response to uric acid also has been shown in VSMC (24, 56).

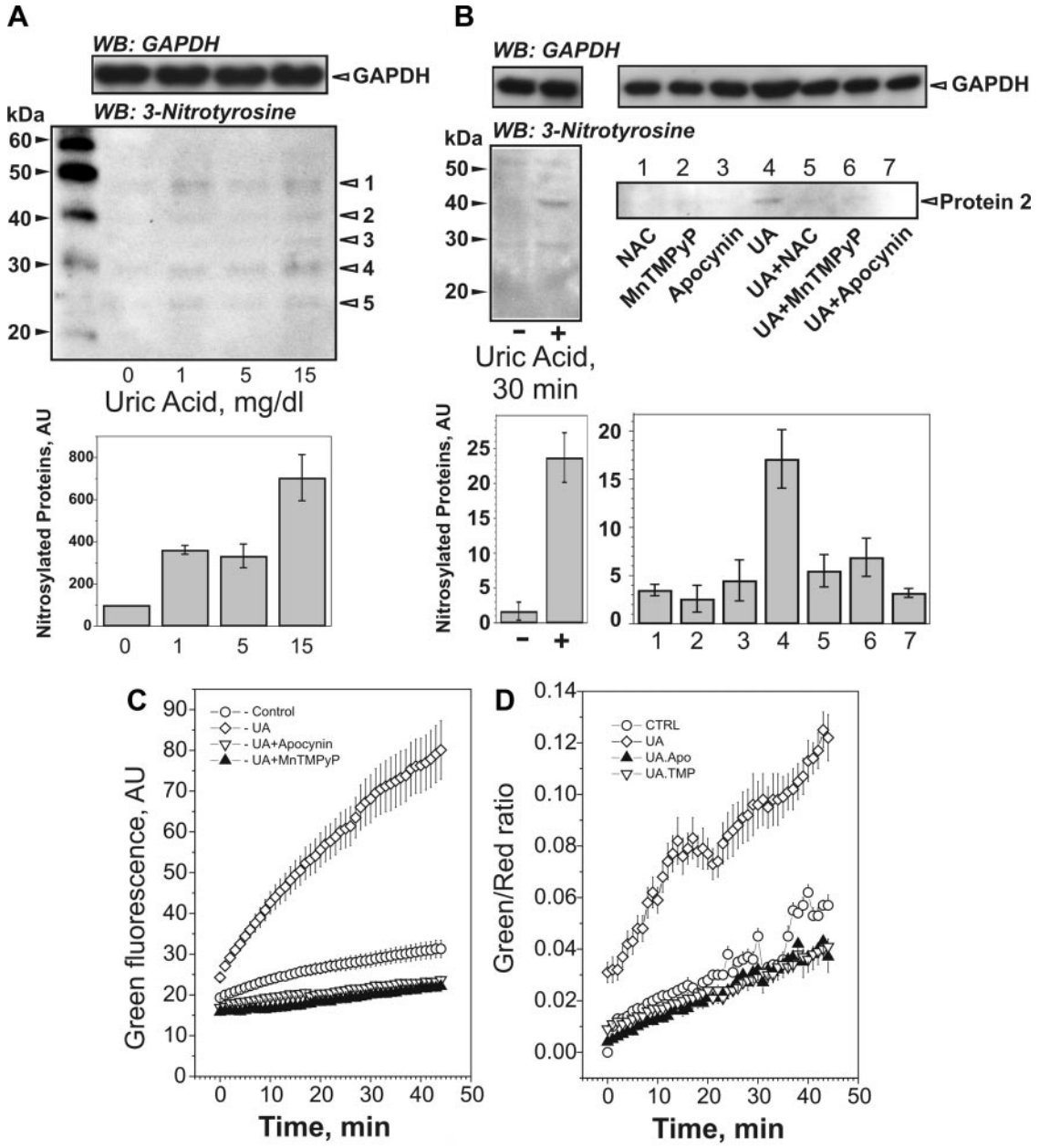

Fig. 8. Urate-induced NOX-dependent protein nitrosylation and lipid peroxidation in adipocytes. *A*: protein nitrosylation in 3T3-L1 cells treated with different concentrations of uric acid present during adipocyte differentiation. *B*: acute effect of uric acid on protein nitrosylation in differentiated adipocytes and its prevention by NAC, superoxide scavenging, and inhibition of NADPH oxidase. Differentiated adipocytes were treated with 15 mg/dl uric acid for varying periods of time or pretreated for 30 min with 10 mM NAC, 200 μM apocynin, or 25 μM MnTMPyP, followed by stimulation with uric acid (15 mg/dl) for 5 min. In *A* and *B*, graphs at *bottom* show the summarized data of densitometric measurements of the abundance of nitrosylated proteins. Values in *A* show the sum of all nitrosylated proteins for each dose of uric acid, normalized to the corresponding control. The effect of uric acid is significant ($P < 0.05$, 1-way ANOVA, $n = 3$). Values in *B* are the optical density of *protein 2*. The effect of uric acid is significant in both cases ($P < 0.05$, *U*-test, $n = 3$). The effects of all inhibitors compared with uric acid-treated cells are significant ($P < 0.05$, *U*-test, $n = 3$). *C*: detection of lipid peroxidation with C11-BODIPY$^{581/591}$. Green fluorescence representing oxidized probe was detected every 60 s for 100 ms after addition of uric acid. *D*: ratiometric analysis of lipid oxidation. The ratio of green to red fluorescence measured every 60 s is shown.

Our results show that uric acid can increase oxidative stress in adipocytes such that local NO is inhibited and protein nitrosylation occurs. We detected an increase in the 3-nitrotyrosine content in several proteins in response to uric acid. The short-term effect of uric acid on the protein nitrosylation was blocked by antioxidants and inhibition of NADPH oxidase, demonstrating that NOX-dependent superoxide overproduction was responsible for protein nitrosylation. 3-Nitrotyrosine is a stable marker of reactive nitrogen species, including peroxynitrite, which forms in a rapid reaction between NO and superoxide with a near-diffusion-controlled rate (10). Peroxynitrite may be especially deleterious for adipocytes, because its diffusion rate in hydrophobic lipid environment is very high (29). Uric acid, indeed, induced lipid peroxidation, which was also prevented by NOX inhibition and superoxide scavenging. In addition, it is known from previous studies that

in the hydrophobic environment, uric acid loses its antioxidant ability (40). In the presence of lipid peroxides, uric acid even becomes a strong prooxidant (3). Thus the intracellular environment of adipocytes, which is predominantly hydrophobic and has a high basal level of ROS, is largely unfavorable for manifestation of the antioxidant properties of uric acid, especially in the case of oxidants such as peroxynitrite. Moreover, uric acid induces intracellular production of superoxide via NOX, followed by formation of ROS and lipid peroxidation, which may further potentiate the chemical prooxidant ability of urate.

The adipose tissue is a source of low-grade inflammation in obesity, and this process plays a major role in the development of insulin resistance and vasculopathy leading to type II diabetes and increasing cardiovascular risk (6, 57). Obesity-associated oxidative stress in the adipose tissue has been recently recognized as a major causative factor for obesity-related inflammation and the metabolic syndrome (13). Uric acid blood levels positively correlate with obesity and body mass index (8, 37, 45) and predict the development of hyperinsulinemia, obesity, and type 2 diabetes (36, 43, 58). Therefore, based on the data presented in this study, hyperuricemia as a persistent condition associated with obesity may be a very important factor contributing to obesity-related oxidative stress.

Our results support previous epidemiological studies and animal models of hyperuricemia, which suggests an involvement of uric acid in the pathogenesis of the metabolic syndrome, and provide a possible molecular mechanism for this role based on the finding that soluble uric acid affects adipocytes directly by inducing NADPH oxidase-dependent oxidative stress. We suggest that hyperuricemia can be one of the causal factors inducing oxidative stress followed by a proinflammatory process and endocrine dysfunction in the adipose tissue, thereby contributing to the pathogenesis of the metabolic syndrome and cardiovascular disease.

GRANTS

This work was supported by National Institutes of Health Grants DK-52121 and HL-68607 (to R. J. Johnson), the Gatorade Research Fund (to Y. Y. Sautin), and an American Lung Association of Florida Grant (to S. Zharikov).

REFERENCES

1. **Abuja PM.** Ascorbate prevents prooxidant effects of urate in oxidation of human low density lipoprotein. *FEBS Lett* 446: 305–308, 1999.
2. **Ames BN, Cathcart R, Schwiers E, Hochstein P.** Uric acid provides an antioxidant defense in humans against oxidant- and radical-caused aging and cancer: a hypothesis. *Proc Natl Acad Sci USA* 78: 6858–6862, 1981.
3. **Bagnati M, Perugini C, Cau C, Bordone R, Albano E, Bellomo G.** When and why a water-soluble antioxidant becomes pro-oxidant during copper-induced low-density lipoprotein oxidation: a study using uric acid. *Biochem J* 340: 143–152, 1999.
4. **Bedard K, Krause KH.** The NOX family of ROS-generating NADPH oxidases: physiology and pathophysiology. *Physiol Rev* 87: 245–313, 2007.
5. **Berg AH, Lin Y, Lisanti MP, Scherer PE.** Adipocyte differentiation induces dynamic changes in NF-κB expression and activity. *Am J Physiol Endocrinol Metab* 287: E1178–E1188, 2004.
6. **Berg AH, Scherer PE.** Adipose tissue, inflammation, and cardiovascular disease. *Circ Res* 96: 939–949, 2005.
7. **Bokoch GM, Knaus UG.** NADPH oxidases: not just for leukocytes anymore! *Trends Biochem Sci* 28: 502–508, 2003.
8. **Bonora E, Targher G, Zenere MB, Saggiani F, Cacciatori V, Tosi F, Travia D, Zenti MG, Branzi P, Santi L, Muggeo M.** Relationship of uric acid concentration to cardiovascular risk factors in young men. Role of obesity and central fat distribution. The Verona Young Men Atherosclerosis Risk Factors Study. *Int J Obes Relat Metab Disord* 20: 975–980, 1996.
9. **Drummen GP, van Liebergen LC, Op den Kamp JA, Post JA.** C11-BODIPY(581/591), an oxidation-sensitive fluorescent lipid peroxidation probe: (micro)spectroscopic characterization and validation of methodology. *Free Radic Biol Med* 33: 473–490, 2002.
10. **Eiserich JP, Patel RP, O'Donnell VB.** Pathophysiology of nitric oxide and related species: free radical reactions and modification of biomolecules. *Mol Aspects Med* 19: 221–357, 1998.
11. **Ellson CD, Gobert-Gosse S, Anderson KE, Davidson K, Erdjument-Bromage H, Tempst P, Thuring JW, Cooper MA, Lim ZY, Holmes AB, Gaffney PR, Coadwell J, Chilvers ER, Hawkins PT, Stephens LR.** PtdIns(3)P regulates the neutrophil oxidase complex by binding to the PX domain of $p40^{phox}$. *Nat Cell Biol* 3: 679–682, 2001.
12. **Engeli S, Janke J, Gorzelniak K, Bohnke J, Ghose N, Lindschau C, Luft FC, Sharma AM.** Regulation of the nitric oxide system in human adipose tissue. *J Lipid Res* 45: 1640–1648, 2004.
13. **Furukawa S, Fujita T, Shimabukuro M, Iwaki M, Yamada Y, Nakajima Y, Nakayama O, Makishima M, Matsuda M, Shimomura I.** Increased oxidative stress in obesity and its impact on metabolic syndrome. *J Clin Invest* 114: 1752–1761, 2004.
14. **Glantzounis GK, Tsimoyiannis EC, Kappas AM, Galaris DA.** Uric acid and oxidative stress. *Curr Pharm Des* 11: 4145–4151, 2005.
15. **Gorin Y, Ricono JM, Kim NH, Bhandari B, Choudhury GG, Abboud HE.** Nox4 mediates angiotensin II-induced activation of Akt/protein kinase B in mesangial cells. *Am J Physiol Renal Physiol* 285: F219–F229, 2003.
16. **Green H, Kehinde O.** An established preadipose cell line and its differentiation in culture. II. Factors affecting the adipose conversion. *Cell* 5: 19–27, 1975.
17. **Hashimoto S, Gon Y, Matsumoto K, Takeshita I, Horie T.** *N*-acetylcysteine attenuates TNF-α-induced p38 MAP kinase activation and p38 MAP kinase-mediated IL-8 production by human pulmonary vascular endothelial cells. *Br J Pharmacol* 132: 270–276, 2001.
18. **Houstis N, Rosen ED, Lander ES.** Reactive oxygen species have a causal role in multiple forms of insulin resistance. *Nature* 440: 944–948, 2006.
19. **Jay D, Hitomi H, Griendling KK.** Oxidative stress and diabetic cardiovascular complications. *Free Radic Biol Med* 40: 183–192, 2006.
20. **Johnson RJ, Kang DH, Cade JR, Rideout BA, Oliver WJ.** Uric acid, evolution and primitive cultures. *Semin Nephrol* 25: 3–8, 2005.
21. **Johnson RJ, Kang DH, Feig D, Kivlighn S, Kanellis J, Watanabe S, Tuttle KR, Rodriguez-Iturbe B, Herrera-Acosta J, Mazzali M.** Is there a pathogenetic role for uric acid in hypertension and cardiovascular and renal disease? *Hypertension* 41: 1183–1190, 2003.
22. **Johnson RJ, Rideout BA.** Uric acid and diet—insights into the epidemic of cardiovascular disease. *N Engl J Med* 350: 1071–1073, 2004.
23. **Kanellis J, Kang DH.** Uric acid as a mediator of endothelial dysfunction, inflammation, and vascular disease. *Semin Nephrol* 25: 39–42, 2005.
24. **Kanellis J, Watanabe S, Li JH, Kang DH, Li P, Nakagawa T, Wamsley A, Sheikh-Hamad D, Lan HY, Feng L, Johnson RJ.** Uric acid stimulates monocyte chemoattractant protein-1 production in vascular smooth muscle cells via mitogen-activated protein kinase and cyclooxygenase-2. *Hypertension* 41: 1287–1293, 2003.
25. **Kang DH, Han L, Ouyang X, Kahn AM, Kanellis J, Li P, Feng L, Nakagawa T, Watanabe S, Hosoyamada M, Endou H, Lipkowitz M, Abramson R, Mu W, Johnson RJ.** Uric acid causes vascular smooth muscle cell proliferation by entering cells via a functional urate transporter. *Am J Nephrol* 25: 425–433, 2005.
26. **Kang DH, Johnson RJ.** Hyperuricemia, gout and the kidney. In: *Diseases of the Kidney* (6th ed.), edited by Schrier RW and Gottschalk CW. Boston, MA: Little Brown, 2005.
27. **Kang DH, Park SK, Lee IK, Johnson RJ.** Uric acid-induced c-reactive protein expression: implication on cell proliferation and nitric oxide production of human vascular cells. *J Am Soc Nephrol* 16: 3553–3562, 2005.
28. **Kapur S, Picard F, Perreault M, Deshaies Y, Marette A.** Nitric oxide: a new player in the modulation of energy metabolism. *Int J Obes Relat Metab Disord* 24, *Suppl* 4: S36–S40, 2000.
29. **Khairutdinov RF, Coddington JW, Hurst JK.** Permeation of phospholipid membranes by peroxynitrite. *Biochemistry* 39: 14238–14249, 2000.
30. **Khosla UM, Zharikov S, Finch JL, Nakagawa T, Roncal C, Mu W, Krotova K, Block ER, Prabhakar S, Johnson RJ.** Hyperuricemia induces endothelial dysfunction. *Kidney Int* 67: 1739–1742, 2005.

31. **Kuzkaya N, Weissmann N, Harrison DG, Dikalov S.** Interactions of peroxynitrite with uric acid in the presence of ascorbate and thiols: implications for uncoupling endothelial nitric oxide synthase. *Biochem Pharmacol* 70: 343–354, 2005.
32. **Lambeth JD.** NOX enzymes and the biology of reactive oxygen. *Nat Rev Immunol* 4: 181–189, 2004.
33. **Mahadev K, Motoshima H, Wu X, Ruddy JM, Arnold RS, Cheng G, Lambeth JD, Goldstein BJ.** The NAD(P)H oxidase homolog Nox4 modulates insulin-stimulated generation of H2O2 and plays an integral role in insulin signal transduction. *Mol Cell Biol* 24: 1844–1854, 2004.
34. **Maples KR, Mason RP.** Free radical metabolite of uric acid. *J Biol Chem* 263: 1709–1712, 1988.
35. **Martyn KD, Frederick LM, von Loehneysen K, Dinauer MC, Knaus UG.** Functional analysis of Nox4 reveals unique characteristics compared to other NADPH oxidases. *Cell Signal* 18: 69–82, 2006.
36. **Masuo K, Kawaguchi H, Mikami H, Ogihara T, Tuck ML.** Serum uric acid and plasma norepinephrine concentrations predict subsequent weight gain and blood pressure elevation. *Hypertension* 42: 474–480, 2003.
37. **Matsuura F, Yamashita S, Nakamura T, Nishida M, Nozaki S, Funahashi T, Matsuzawa Y.** Effect of visceral fat accumulation on uric acid metabolism in male obese subjects: visceral fat obesity is linked more closely to overproduction of uric acid than subcutaneous fat obesity. *Metabolism* 47: 929–933, 1998.
38. **Matute JD, Arias AA, Dinauer MC, Patino PJ.** p40^{phox}: the last NADPH oxidase subunit. *Blood Cells Mol Dis* 35: 291–302, 2005.
39. **Miyazaki H, Sekine T, Endou H.** The multispecific organic anion transporter family: properties and pharmacological significance. *Trends Pharmacol Sci* 25: 654–662, 2004.
40. **Muraoka S, Miura T.** Inhibition by uric acid of free radicals that damage biological molecules. *Pharmacol Toxicol* 93: 284–289, 2003.
41. **Nakagawa T, Hu H, Zharikov S, Tuttle KR, Short RA, Glushakova O, Ouyang X, Feig DI, Block ER, Herrera-Acosta J, Patel JM, Johnson RJ.** A causal role for uric acid in fructose-induced metabolic syndrome. *Am J Physiol Renal Physiol* 290: F625–F631, 2006.
42. **Nakagawa T, Tuttle KR, Short RA, Johnson RJ.** Hypothesis: fructose-induced hyperuricemia as a causal mechanism for the epidemic of the metabolic syndrome. *Nat Clin Pract Nephrol* 1: 80–86, 2005.
43. **Nakanishi N, Okamoto M, Yoshida H, Matsuo Y, Suzuki K, Tatara K.** Serum uric acid and risk for development of hypertension and impaired fasting glucose or type II diabetes in Japanese male office workers. *Eur J Epidemiol* 18: 523–530, 2003.
44. **Oda M, Satta Y, Takenaka O, Takahata N.** Loss of urate oxidase activity in hominoids and its evolutionary implications. *Mol Biol Evol* 19: 640–653, 2002.
45. **Ogura T, Matsuura K, Matsumoto Y, Mimura Y, Kishida M, Otsuka F, Tobe K.** Recent trends of hyperuricemia and obesity in Japanese male adolescents, 1991 through 2002. *Metabolism* 53: 448–453, 2004.
46. **Oliveira HR, Verlengia R, Carvalho CR, Britto LR, Curi R, Carpinelli AR.** Pancreatic β-cells express phagocyte-like NAD(P)H oxidase. *Diabetes* 52: 1457–1463, 2003.
47. **Pap EH, Drummen GP, Winter VJ, Kooij TW, Rijken P, Wirtz KW, Op den Kamp JA, Hage WJ, Post JA.** Ratio-fluorescence microscopy of lipid oxidation in living cells using C11-BODIPY(581/591). *FEBS Lett* 453: 278–282, 1999.
48. **Price KL, Sautin YY, Long DA, Zhang L, Miyazaki H, Mu W, Endou H, Johnson RJ.** Human vascular smooth muscle cells express a urate transporter. *J Am Soc Nephrol* 17: 1791–1795, 2006.
49. **Rao GN, Corson MA, Berk BC.** Uric acid stimulates vascular smooth muscle cell proliferation by increasing platelet-derived growth factor A-chain expression. *J Biol Chem* 266: 8604–8608, 1991.
50. **Reaven GM.** The kidney: an unwilling accomplice in syndrome X. *Am J Kidney Dis* 30: 928–931, 1997.
51. **Santos CX, Anjos EI, Augusto O.** Uric acid oxidation by peroxynitrite: multiple reactions, free radical formation, and amplification of lipid oxidation. *Arch Biochem Biophys* 372: 285–294, 1999.
52. **Sheppard FR, Kelher MR, Moore EE, McLaughlin NJ, Banerjee A, Silliman CC.** Structural organization of the neutrophil NADPH oxidase: phosphorylation and translocation during priming and activation. *J Leukoc Biol* 78: 1025–1042, 2005.
53. **Stocker R, Keaney JF Jr.** Role of oxidative modifications in atherosclerosis. *Physiol Rev* 84: 1381–1478, 2004.
54. **Taille C, El-Benna J, Lanone S, Boczkowski J, Motterlini R.** Mitochondrial respiratory chain and NAD(P)H oxidase are targets for the antiproliferative effect of carbon monoxide in human airway smooth muscle. *J Biol Chem* 280: 25350–25360, 2005.
55. **Usatyuk PV, Vepa S, Watkins T, He D, Parinandi NL, Natarajan V.** Redox regulation of reactive oxygen species-induced p38 MAP kinase activation and barrier dysfunction in lung microvascular endothelial cells. *Antioxid Redox Signal* 5: 723–730, 2003.
56. **Watanabe S, Kang DH, Feng L, Nakagawa T, Kanellis J, Lan H, Mazzali M, Johnson RJ.** Uric acid, hominoid evolution, and the pathogenesis of salt-sensitivity. *Hypertension* 40: 355–360, 2002.
57. **Wellen KE, Hotamisligil GS.** Inflammation, stress, and diabetes. *J Clin Invest* 115: 1111–1119, 2005.
58. **Yoo TW, Sung KC, Shin HS, Kim BJ, Kim BS, Kang JH, Lee MH, Park JR, Kim H, Rhee EJ, Lee WY, Kim SW, Ryu SH, Keum DG.** Relationship between serum uric acid concentration and insulin resistance and metabolic syndrome. *Circ J* 69: 928–933, 2005.